

Sedimentation analysis of small ice crystals by Lattice Boltzmann Method

Juan P. Giovacchini^{*1,2}

¹Depto Mecánica Aeronáutica, Instituto Universitario Aeronáutico, Córdoba, Argentina.

²Instituto de Física Enrique Gaviola (CONICET), Córdoba, Argentina.

Abstract

Lattice Boltzmann Method (LBM) is used to simulate and analyze the sedimentation of small ($16-80\ \mu m$) ice particles in the atmosphere. We are specially interested in evaluating the terminal falling velocity for two ice particle shapes: columnar ice crystals and six bullet-rosettes ice polycrystal. The main objective in this paper is to investigate the LBM suitability to solve ice crystal sedimentation problems, as well as to evaluate these numerical methods as a powerful numerical tool to solve these problems for arbitrary ice crystal shapes and sizes. LBM results are presented in comparison with laboratory experimental results and theoretical proposals well known in the literature. The numerical results show good agreement with experimental and theoretical results for both geometrical configurations.

1 Introduction

Ice crystals with a variety of shape, size and mass are present in clouds. The properties of these crystals are markedly dependent on the temperature and other properties of the atmosphere (Ryan *et al.*, 1976; Heymsfield & Iaquinta, 2000). A classification of ice crystals with a description of crystal shapes, size and mass can be found in Magono & Lee (1966); Ryan *et al.* (1976); Heymsfield & Iaquinta (2000); Bailey & Hallett (2009).

Certain atmospheric and cloud behaviors are characterized by parameters related to the ice particle dynamics for different shapes and sizes (Eidhammer *et al.*, 2014). A precise estimation of ice crystals falling velocity is required to quantitatively determine their evolution in the atmosphere. The knowledge of the falling velocity is necessary for the simulation of ice water paths and for the determination of cloud boundaries

^{*}Electronic address: giovacchini@famaf.unc.edu.ar

(Khvorostyanov & Curry, 2002). Also it is used for the study of microphysical process in clouds and for climate modeling (Kajikawa, 1973; Khvorostyanov & Curry, 2002; Bürgesser *et al.*, 2016).

The need for more accurate theoretical models to simulate clouds has increased the requirement of more detailed measurements of relationships between the settling velocity, masses, and dimensions for a large spectrum of ice crystal types. A precise determination of these relationships allow us to obtain accurate parameterizations of the settling velocity of cloud particles. These parametrizations are essential to have an accurate simulation of cloud in general circulation models (GCMs) of precipitation amount, cloud dissipation and cloud optical properties (Khvorostyanov & Curry, 2002; Heymsfield & Iaquinta, 2000).

Although there have been many proposals in literature, the ice crystal sedimentation in the atmosphere has not been completely characterized (Heymsfield & Iaquinta, 2000; Westbrook, 2008; Heymsfield & Westbrook, 2010). There are analytical solutions that precisely determine the sedimentation falling velocity for spheres particles. Due to the large variety of shapes, sizes and masses of ice crystals, and the range of Reynolds numbers involved in these problems, there is no precise analytical estimation to predict the falling velocity for shapes other than spheres. Many works in literature (Böhm, 1989, 1992; Mitchell, 1996; Mitchell & Heymsfield, 2005; Heymsfield & Iaquinta, 2000; Khvorostyanov & Curry, 2002, 2005; Westbrook, 2008; Heymsfield & Westbrook, 2010) provide schemes to parameterize the ice crystal masses, shapes and size to predict the settling velocity. Ice particle terminal velocities are often calculated theoretically or experimentally by determining a relationship between the Reynolds number (Re), and the Best (or Davis) number, (X) (Jayaweera & Cottis, 1969; Jayaweera & Ryan, 1972; Böhm, 1989; Mitchell, 1996).

There are a number of experimental works in which the most important variables are measured. Terminal velocity, mass and size have been measured for various ice particle types. These datasets are obtained from laboratory measurement and observations of real ice particles falling through the atmosphere. Some well known experimental datasets can be found in Jayaweera & Cottis (1969); Jayaweera & Ryan (1972); Kajikawa (1973); Locatelli & Hobbs (1974); Michaeli (1977); Bürgesser *et al.* (2016).

The proposals by Böhm (1989, 1992); Mitchell (1996); Mitchell & Heymsfield (2005); Khvorostyanov & Curry (2002, 2005) have shown quite good approximations to the falling speed of ice particles for $Re \gg 1$. These proposals proved to be in good agreement with experimental data for a variety of particle types. However Westbrook *et al.* (2008) showed that for viscous flow regimes ($Re \ll 1$) these formulations overestimate the crystal falling velocity. Westbrook (2008), using the approximation of Hubbard & Douglas (1993) with results from Westbrook *et al.* (2008), give an estimate for the sedimentation rate of small ice crystals whose maximum dimension is smaller

than $100\mu\text{m}$. This estimate for columnar ice crystals is in agreement with most experimental data (within 20%).

A complete review of the main theoretical approximation that have been proposed and many experimental results can be found in (Mitchell, 1996; Mitchell & Heymsfield, 2005; Heymsfield & Iaquinta, 2000; Khvorostyanov & Curry, 2002, 2005; Heymsfield & Iaquinta, 2000; Heymsfield & Westbrook, 2010); also a lots of relevant references are presented in these works.

The sedimentation of an ice crystal in the atmosphere is a fluid mechanical problem that can be modeled as a rigid body moving immersed in a fluid flow. This rigid body moves under the action of its own weight, buoyancy force and interacting with others crystals and with the fluid that surrounds it.

Given a characterization for the shape, size and mass density of the crystals, together with its atmospheric habitat, it is possible to completely determine the dynamical behavior of the crystals by using some adequate computational fluid dynamic (CFD) method. Having an accurate numerical method to solve these problems allows us in turn to test and to improve the parametrization laws, and to compute the settling velocities for sizes, shapes and masses for which experimental data are not available. Also, the sensitivity of the problem to different parameters can be studied numerically.

To the knowledge of the author, there are no numerical results that describe appropriately the dynamics of ice crystals in the atmosphere.

The LBM is a CFD method that proved to be successful to treat multiple problems involving both compressible and incompressible flows on simple and complex geometrical settings. In particular the LBM provide a simple way for treating accurately the flow surrounding an immersed body, in arbitrary movement, with no regular geometry. For a complete modern review of this topic see Aidun & Clausen (2010). The behavior of particles in sedimentation have been analyzed using LBM in a variety of problems (Ladd, 1994*a,b*; Aidun & Lu, 1995; Aidun *et al.*, 1998; Xia *et al.*, 2009).

In this paper we use LBM to study the dynamical behavior of ice crystals with two different shapes: simple columns and six bullet polycrystal (a combination of columns or bullets). In particular, the ice crystal settling velocity is obtained numerically for both shapes in a range of masses and sizes (characteristic lengths of $l = 16 - 80\mu\text{m}$). The LBM results for the fluid mechanical problems are obtained in a pure viscous regime ($Re \ll 1$). This is the flow regime of the smallest particles falling in a cloud. The accuracy in the LBM to treat this problem is evaluated by comparison with some well known experimental data in literature (Jayaweera & Ryan, 1972; Kajikawa, 1973; Michaeli, 1977; Bürgesser *et al.*, 2016), and with theoretical proposal from (Mitchell, 1996; Mitchell & Heymsfield, 2005; Khvorostyanov & Curry, 2002, 2005) and Westbrook (2008).

In order to prove the correctness and accuracy of the proposed LBM algorithm, two fluid mechanical problems at low Reynolds number were

tested. The idea of these benchmarks is to test our algorithm in translational and rotational problems, within the Re regime that include the ice crystal sedimentation problems.

The paper is organized as follows: In section 2 we present the basic equations of the LBM, introduce notation and some details about the boundary conditions methods, force evaluation, and grid refinement techniques. In section 3 we evaluate the correctness of the proposed LBM algorithm to solve two benchmarks, *sphere sedimentation in a square duct* (section 3.1) and *pure rotation of rigid bodies in Couette flow* (section 3.2), well known in the literature. In section 4 the sedimentation of ice crystals in the atmosphere is solved using LBM. Numerical results for *columnar ice crystals* and *six bullet-rosette ice polycrystals* are showed in sections 4.1 and 4.2 respectively. In section 5 conclusions and discussions are presented.

2 The lattice Boltzmann method

In this section we present the basic equations of the LBM, introduce notation and the main concepts we use along the paper.

In addition to the lattice Boltzmann equation that govern the physics of the bulk fluid; one needs to prescribe a method to apply boundary conditions, to evaluate the fluid force on a body and to implement grid refinement where necessary. In the next sections we briefly review these topics.

2.1 Lattice Boltzmann equation

The numerical results in this paper are obtained by solving the lattice Boltzmann equation (*LBE*) (He & Luo, 1997b; Succi, 2001; Wolf-Gladrow, 2000), a particular phase-space and temporal discretization of the Boltzmann equation (*BE*) (Harris, 2004; Sone, 2007).

The BE governs the time evolution of the single-particle distribution function $f(\mathbf{x}, \boldsymbol{\xi}, t)$, where \mathbf{x} and $\boldsymbol{\xi}$ are the position and velocity of the particle in phase space. The LBE is a discretized version of the BE, where \mathbf{x} takes values on a uniform grid (the lattice), and $\boldsymbol{\xi}$ is not only discretized, but also restricted to a finite number Q , (the number of discrete velocities in the model) of values (He & Luo, 1997b). In an isothermal situation and in the absence of external forces, like gravity, the LBE can be written as:

$$\mathbf{f}(\mathbf{x} + \mathbf{c}_i \delta t, t + \delta t) = \mathbf{f}(\mathbf{x}, t) + \boldsymbol{\Omega}(\mathbf{f}(\mathbf{x}, t) - \mathbf{f}^{eq}(\mathbf{x}, t)) \quad (1)$$

Here $f_i = f_i(\mathbf{x}, t)$ is the i -th component of the discretized distribution function $\mathbf{f}(\mathbf{x}, t)$ at the lattice site \mathbf{x} , time t , and discrete velocity \mathbf{c}_i . The function $\mathbf{f}^{eq}(\mathbf{x}, t)$ is a discrete version of the equilibrium distribution function (He & Luo, 1997b) and $\boldsymbol{\Omega}$ is a linearized collision operator. In our simulations we use a simple relaxation time model (*SRT*), a simplified approx-

imation of Ω that follows from the Bhatnagar, Gross, and Krook (BGK) (Bhatnagar *et al.*, 1954) approximation with relaxation time τ .

In compressible-flow models the lattice constant δx , that separate two nearest neighbor nodes, and the time step δt are related with the speed of sound $c/\sqrt{3}$ by $\delta x = c\delta t$. In incompressible-flow models, the same relation between δx and δt holds, but the constant c is no longer related to the speed of sound. The coordinates of a lattice node are denoted by \mathbf{x}_A , where the integer multi index $A = (j, k, l)$ (or, $A = (j, k)$ in the two-dimensional case) denotes a particular site in the lattice.

The macroscopic quantities such as the fluid mass density $\rho(\mathbf{x}, t)$, and velocity $\mathbf{u}(\mathbf{x}, t)$, are obtained, in Boltzmann theory, as marginal distributions of f and ξf when integrating over ξ . In LBM this integrals are approximated by proper quadratures. Specific values of c_i 's and ω_i 's, $i = 0, 1, \dots, Q-1$, are made so that these quadratures give exact results for the ξ -moments of order 0, 1 and 2 (He & Luo, 1997b; Wolf-Gladrow, 2000). We have

$$\rho(\mathbf{x}_A, t) = \sum_{i=0}^{Q-1} f_i(\mathbf{x}_A, t), \quad (2)$$

and

$$\rho \mathbf{u}(\mathbf{x}_A, t) = \sum_{i=0}^{Q-1} \mathbf{c}_i f_i(\mathbf{x}_A, t). \quad (3)$$

In the simulations we present in this paper, we are interested in incompressible flow problems, where we modify Eq. 3 according to the quasi-incompressible approximation presented in (He & Luo, 1997a). In this approximation ρ is replaced by ρ_0 , a constant fluid mass density.

A single time step of the discrete evolution equation 1 is frequently written as a two-stage process

$$\hat{f}_i(\mathbf{x}_A, t) = f_i(\mathbf{x}_A, t) - \frac{1}{\tau} \left(f_i(\mathbf{x}_A, t) - f_i^{eq}(\mathbf{x}_A, \rho, \mathbf{u}, t) \right), \quad (4)$$

and

$$f_i(\mathbf{x}_A + \mathbf{c}_i \delta t, t + \delta t) = \hat{f}_i(\mathbf{x}_A, t). \quad (5)$$

The computation of \hat{f}_i on the whole lattice, Eq. 4, is called the *collision step*, while the computation of f_i at $t + \delta t$, Eq. 5, on the whole lattice is called *streaming step*.

We refer to the lattice Boltzmann models with the standard notation $DmQn$, where m is the number of space dimensions of the problem, and n is the number of discrete velocities. Also we add an i at the end to indicate that we use a quasi-incompressible approximation, $DmQni$.

2.2 Boundary conditions

The problems we are interested in are those in which rigid bodies move inside an unbounded fluid domain. Because the impossibility to model an infinite fluid domain, we have to restrict the problem to a finite computational fluid domain. The size of the computational fluid domain has to be a compromise between minimizing the computational work—the smaller the size the better, and minimizing the undesirable effect of the boundary conditions—the larger the domain the better.

The computational fluid domain is a block of fluid bounded by regular borders. The rigid bodies that move inside the domain are described by geometries as required.

The flow in the interior of the domain is computed by solving the LBE. Close to the boundaries a special treatment is used so that the flow obeys the physical boundary conditions. In the present work, we use both Dirichlet and outflow open-boundary conditions (convective boundary conditions or Sommerfeld like). The correct imposition of the boundary conditions on arbitrary boundary geometries, like the boundary of rigid bodies, has been one of the main issues in LBM.

To impose Dirichlet boundary conditions, for the velocity or pressure, on a regular boundary which is coincident with the grid, we use the method proposed in Zou & He (1997). These regular boundaries are adequately represented by linked lattice nodes.

To impose Dirichlet conditions for the velocity on boundaries of arbitrary shape we use the method proposed by Bouzidi *et al.* (2001). We also use the method shown in Mei *et al.* (1999) and obtain no significant differences in the results.

In order to reduce the length of the numerical flow domain we apply a convective, or Sommerfeld like, boundary conditions on the open boundaries of the domain. These boundary conditions allow us to model a long or quasi-infinite physical domain with a reduced computational domain. These type of conditions have been extensively applied in computational fluid mechanics. We make a particular implementation of convective boundary condition in the LBM context. More details about our implementation are given in section 2.2.1.

2.2.1 Outflow open-boundary conditions

The outflow open-boundary conditions allow us to represent a long or quasi-infinite physical domain by a finite computational domain.

In many fluid mechanical problems on a large, quasi-infinite fluid domain, the region in which the velocity gradients, viscosity and inertial forces are significant is rather small. It is a challenge to adequately represent such a fluid mechanical problem on a bounded, as small as possible, computational

domain in such a way that the interesting physics is captured accurately and at the same time the computational cost is reduced significantly. Strictly speaking, one needs to apply convenient boundary conditions at the finitely close computational boundaries so that these conditions do not affect the physical behavior of the flow in the interior or ruin the intrinsic LBM accuracy.

There are different approaches in the literature to treat the outflow open-boundary conditions in the LBM context. We can divide these approaches in at least two categories, the ones based on mesoscopic variables (Yu *et al.*, 2005; Chikatamarla *et al.*, 2006) and the ones based on macroscopic variables (Aidun *et al.*, 1998; Yang, 2007; Junk & Yang, 2008; Yang, 2013). The latter are generally extensions of boundary conditions extensively applied in classical methods (Finite Difference (*FD*), Finite Volume (*FV*) and Finite Element (*FE*) methods) of computational fluid mechanics (*CFD*) to solve the Navier-Stokes (*NS*) equations.

We are mainly interested in non-stationary quasi-incompressible problems. In the LBM context the convective boundary condition (CBC) proposed in Yang (2013) to treat outflow open-boundaries has shown acceptable results in these kind of problems. Also, in Sohankar *et al.* (1998) it is shown that CBC gives better results than Neumann boundary conditions (*NBC*) when using *FV* methods to solve the incompressible *NS* equation.

The *NBC* are based on macroscopic variables, and were also tested in LBM (Aidun *et al.*, 1998; Yang, 2007; Junk & Yang, 2008; Yang, 2013). The results presented in Yang (2007, 2013) show that CBC are a better option than *NBC* in non-stationary problems. These works show that *NBC* introduce undesirable perturbations in the fluid domain, specially in non-stationary problems.

In our numerical tests we use CBC to fix the velocity in the outflow open-boundaries. To complete the CBC method we use some Dirichlet boundary condition method to fix the unknown mesoscopic (f' 's) variables that have to satisfy the macroscopic CBC.

The CBC is defined as:

$$\frac{\partial \phi}{\partial t} + \bar{v} \mathbf{n} \cdot \nabla \phi(\mathbf{x}, t) = 0 \quad , \quad \mathbf{x} \in \partial \Gamma, t \in [0, T] \quad (6)$$

where ϕ is a velocity or pressure function, and \bar{v} is a reference velocity that have to be defined adequately. $\partial \Gamma$ is the boundary of the fluid domain Γ , and \mathbf{n} is the outward normal vector in $\partial \Gamma$. In our numerical implementation CBC are applied on straight, grid-coincident boundaries only.

To show the implementation of the CBC, we consider as an example a boundary with normal vector $\mathbf{n} = (1, 0, 0)$. Given the LBE solution at time t , 6 gives, for $\phi = \mathbf{u}$,

$$\mathbf{u}(\mathbf{x}, t + \delta t) \approx \mathbf{u}(\mathbf{x}, t) - \frac{\bar{v} \delta t}{2h} (\mathbf{u}(\mathbf{x} - 2h\mathbf{n}, t) - 4\mathbf{u}(\mathbf{x} - h\mathbf{n}, t) + 3\mathbf{u}(\mathbf{x}, t)) \quad , \quad (7)$$

where we have approximated the space derivative by a second order accurate, backward difference operator and the time derivative by a first order accurate, forward difference operator.

From equation 7 the velocity $\mathbf{u}(\mathbf{x}, t + \delta t)$ that satisfy the CBC can be determined. Knowing the boundary velocity at $t + \delta t$ some Dirichlet boundary condition can be used to determine the corresponding mesoscopic variables.

We implement the CBC method coupled with the proposal of Zou & He (1997) to impose the boundary velocity determined from equation 7.

Equation 7 is incomplete until we provide a prescription for the value of \bar{v} . Various criteria can be found in the literature to do this. Yang (2013) sets this quantity equal to the mean velocity on the outflow open convective boundary. Sohankar *et al.* (1998) sets \bar{v} equal to the upstream free velocity $\|\mathbf{u}_\infty\|$ with some additional conditions to ensure mass conservation in the fluid domain. Mass conservation problems are also observed in the case of Yang (2013).

In our implementation we set \bar{v} as a constant: the upstream mean velocity. We have observed, by performing typical benchmark tests, that mass is acceptably conserved by the resulting scheme.

2.3 Forces evaluation

It is of crucial importance, in many applications that involve moving bodies surrounded by a fluid flow, to have a good method or algorithm to compute the flow force and torque acting on the bodies. By good we mean a method that is simple to apply, that is accurate and fast, so as not to spoil the efficiency of the flow computing method. The accuracy in the determination of the force and torque acting on a moving body directly affects the body's movement. For a review of LBM methods that involve flow force evaluation on suspended particles we refer to Section 6 of Aidun & Clausen (2010) and references therein.

The classical way to compute forces, and so torque, on submerged bodies is via the computation and integration of the stress tensor on the surface of the body. In LBM the stress tensor is a local variable, its computation and extrapolation from the lattice to the surface is computationally expensive, which ruins the efficiency of the LBM. However, this method is widely used in LBM (Inamuro *et al.*, 2000; Xia *et al.*, 2009; Li *et al.*, 2004).

An standard method to evaluate forces on submerged bodies in LBM is the *momentum exchange (ME)*, introduced firstly by Ladd (1994a,b) in LBM applications. The ME algorithm is specifically designed and adapted to LBM; it is therefore more efficient than stress integration from the computational point of view.

Some improvements to Ladd proposal have been introduced in (Aidun & Lu, 1995; Aidun *et al.*, 1998; Mei *et al.*, 2002), and different approaches to improve the methods in problems with moving bodies were made (Wen *et al.*,

2012, 2014; Giovacchini & Ortiz, 2015). In this work, force and torque are evaluated by using the methods presented in Giovacchini & Ortiz (2015).

The motion of each body is determined by solving the Newton’s equations of motion with rotations formulated using quaternions (Goldstein *et al.*, 2001). The forces acting over bodies are given by the fluid flow forces, weight and buoyancy forces. To integrate in time we use Euler Forward numerical scheme, which is first order accurate as the LBM method itself.

2.4 Grid refinement method

Many problems in fluid mechanics are such that big gradients of the fluid variables appear only in regions which are small as compared with the whole computational domain. To resolve well the space variations of the fluid variables one needs a grid size which is small enough.

In LBM a simple lattice is a Cartesian grid of equispaced nodes. The distance between two nearest neighbor nodes, the grid size, is δx . For a real problem, the computational domain is covered by an arrangement of grids. This arrangement can be as simple as a unique lattice—or block grid—with a single size δx , or a complex arrangement of grids with different grid sizes.

In a problem with more or less uniform space variations all over, a single block grid that covers the whole computational domain may be suitable. In a problem where high space variations occur in a small region, a small grid size needs to be used in that region. But using this small grid size on the whole computational domain would be a waste of computational effort. The right thing to do is to use an arrangement of grids with different grid sizes. The methods to integrate various grid blocks with different grid sizes into a single computational domain are known as grid refinement methods.

In LBM there are at least two grid refinement methods: *multi-grid method* (MG) (Filippova & Hnel, 1998*b,a*) and *multi-domain method* (MD) (or multi-block) (Yu *et al.*, 2002; Lagrava *et al.*, 2012). In the MG method, a grid block with small grid size is always superimposed to a grid block with larger grid size. Several layers of grids can be superimposed in this way. In MD method the grids with different grid sizes overlap just in a selected set of lattice nodes. This overlapping occurs only on a small region with two adjacent grid blocks of different grid sizes, see (Yu *et al.*, 2002; Lagrava *et al.*, 2012).

In this work we use MD methods. We select this method because it has better numerical performance and lesser memory requirement than MG method. A disadvantage of the MD method, though, is that its implementation is more complex than that of MG where some additional grids are used as interface to interchange data between different levels of grid size.

We use a priori refinement method. This means that we chose the arrangement of refined grids in the domain before solving the fluid problem, and this arrangement is fixed in time. This last characteristic becomes the

main numerical performance limitation of our method.

In non-stationary fluid problems the smallest scales to solve and its position within the fluid domain are not easy to predict. A priori refinement methods are not the most efficient option in non-stationary fluid problems, one frequently needs to implement *adaptive refinement methods* (Tölke *et al.*, 2006; Fakhari & Lee, 2014). This adaptive methods are able to change the refined grids arrangement at run time.

3 Benchmark tests for the correctness of LBM algorithm

In this section we show LBM results for two fluid mechanical problems well known in the literature. Our purpose is to test the correctness of the proposed LBM algorithm to solve problems at low Reynolds numbers as those in ice crystals sedimentation.

The rigid body equations of movement are independently solved for translations and rotations, they are only coupled through the fluid forces. Therefore we chose two particular problems, with well known results, to test pure translations and pure rotations.

3.1 Sphere sedimentation in a square duct

We are interested in the problem of an sphere sedimenting inside a square section duct full of a viscous fluid. We are particularly interested in the determination of the sphere's terminal falling velocity v_s . In figure 1a) we show a scheme of the problem configuration.

We compute v_s for different values of the relation $\frac{d}{L}$ between the sphere's diameter d and the length L of the square cross section. We are looking for the relation $\frac{v_s}{v_T}$, as a function of $\frac{d}{L}$, where v_T is the sphere's terminal falling velocity in an unbounded fluid domain. The ratio $\frac{v_s}{v_T}$ is commonly named *wall correction factor*.

The terminal falling velocity is the stationary velocity that a body (sphere) reaches in a sedimentation process; the body and viscous forces are equal in magnitude in this stationary regime. v_T is obtained from a Stokes flow regime defined by

$$v_T = \frac{2}{9} r^2 \frac{g}{\nu} \left(\frac{\rho_e}{\rho_f} - 1 \right), \quad (8)$$

with $r = \frac{d}{2}$, ρ_e the sphere's material density, ρ_f the fluid's density and ν the fluid's kinematic viscosity. The value of v_T given by equation 8 is an adequate estimation if the fluid flow is consistent with Stoke problem hypothesis (White, 2005).

The sphere sedimenting in a square section duct is a problem analyzed in the literature. Aidun *et al.* (1998) numerically determine the wall correction

factor using the LBM, and Miyamura *et al.* (1981) experimentally analyze this problem.

Aidun *et al.* (1998) evaluate the wall correction factor for different configurations and compare their results with the experimental results presented in Miyamura *et al.* (1981). Aidun *et al.* (1998) use a quasi-incompressible LBM and some particular boundary conditions and forces evaluation method.

Miyamura *et al.* (1981) experimentally study the wall interference effects over the sphere terminal velocity. They test the wall correction factor for different sphere diameters and duct cross section configuration. As a main result they show a curve fitting to the obtained experimental data in those problems. We will use this fitting equation to compare with our LBM results.

In figure 1a) we show an schematic arrangement of grids refinement and the sphere placed in its initial position at $t = 0$ s. The refinement region is placed from H_1 to $H_1 + H_2$, a bounded fluid region where will take place the rigid body displacement.

We use a computational domain of length H to represent a quasi-infinite physical one. We made several numerical test for different domain configurations. We look for the best combination of length domains (H, H_1 , and H_2) and sphere placement (h) that produce acceptable results and minimize the computational cost. We refer as acceptable results, those results uninfluenced by the computational domain length H . From the numerical test we found that acceptable results require $\frac{H}{L} \geq 12$.

In figure 1b) we show the obtained LBM numerical results along with the polynomial fitting from the experimental data presented in (Miyamura *et al.*, 1981). We use in our computations $L = 0.01$ m and $H = 12L$. The refinement region with length $H_2 = 2L$ is placed at $H_1 = 6L$ from the bottom wall.

The results showed in figure 1b) are obtained using the $D3Q15i$ lattice Boltzmann model with a domain discretization of $61 \times 121 \times 61$ for the fine grid.

Dirichlet boundary conditions are set over all the domain's walls. In the horizontal top wall (see figure 1a)) the boundary velocity is set according to the convective boundary condition presented in section 2.2.1. Over the sphere surface we set the velocity boundary condition using methods for non regular boundaries as presented in Bouzidi *et al.* (2001).

We evaluate the wall correction factor for eight relations $\frac{d}{L}$ ranging from 0.1 to 0.8, with diameters $d = 1$ mm to $d = 8$ mm respectively. The sphere is initially placed in the cross sectional center at $h = 7L$ from the bottom wall domain. As initial condition we set an equal and homogeneous velocity \mathbf{u}_0 in the fluid flow domain. The numerical tests consist in releasing a sphere in a particular way, as explained below, from its initial position h with velocity \mathbf{u}_0 at $t = 0$ s. The initial velocity \mathbf{u}_0 is approximately equal to and opposite in direction to the terminal falling velocity v_s of the rigid body inside the square duct.

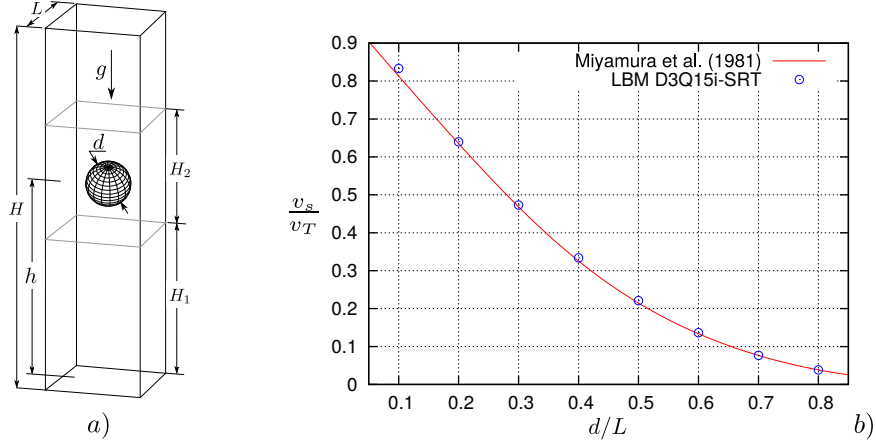


Figure 1: a) Geometrical configuration scheme. H_2 is the length of the refined region starting at height H_1 as measured from the bottom domain wall. b) Wall correction factor $\frac{v_s}{v_T}$ vs. $\frac{d}{L}$ for a sphere falling inside a square cross section duct. The continuous line is the polynomial fitting of experimental data from (Miyamura *et al.*, 1981).

There are at least two main reasons to analyze the problem in a constant velocity frame. On the one hand, being the rigid body at an approximately constant position, relative to the computational fluid domain, reduces the region of refinement and simplifies the refinement algorithm, since we can keep the refinement region fixed (no dynamical refinement process is necessary). On the other hand, the constant velocity fluid domain with adequate boundary conditions allows us to reduce the length of the domain. The rigid body is roughly static in the computational fluid domain length and we can fix the minimal appropriate relation $\frac{H}{L}$ so that the rigid body stays in the refined region.

We apply a particular initialization procedure so that the body stays in a prefixed gap (refined region). We initially impose a fictitious external force during some time interval so that the relative velocity between the rigid body and the fluid domain is approximately v_s . After this time interval the rigid body is left to move freely in the fluid domain. Because the application of the artificial initial force there is a fictitious transient which we are not interested in.

Once the sphere reaches the stationary regime (after $t > t_s$), the terminal falling velocity v_s is considered equal to the sphere stationary falling velocity.

The Reynolds number (Re) in our tests are in the range $0.0005 \leq Re \leq 0.39$, while the Re range in (Aidun *et al.*, 1998) and (Miyamura *et al.*, 1981) are $0.2 \leq Re \leq 0.6$ and $0.000241 \leq Re \leq 0.699$ respectively.

The results we have obtained, presented in figure 1b), have an acceptable correlation with those experimentally obtained in (Miyamura *et al.*, 1981).

Our results are close to the experimentally adjusted curve in the whole $\frac{d}{L}$ -range.

The largest differences between experimental and LBM results are observed for $\frac{d}{L} = 0.1$ which is particularly noticed for spheres of small radii. The reason for these differences can be that the discretization is not fine enough, since the domain discretization is kept constant for all $\frac{d}{L}$ relations.

Our numerical results show a better approximation to the experimental results than those presented in (Aidun *et al.*, 1998) for the same problem.

The pure translation assumption is justified by the angular displacement results. If flow instabilities are present, like typically those from high Reynolds number problems, this statement is not longer true.

3.2 Pure rotation of rigid bodies in Couette flow

In this section we want to test our LBM algorithm for describing pure rotation of rigid bodies immersed in a fluid flow. Particularly, two rigid bodies (2D and 3D) immersed in a Couette flow are analyzed.

Our main interest is to benchmark our LBM results with those presented by Aidun *et al.* (1998) and Qi & Luo (2003). We test two rigid body configurations: an ellipse and an ellipsoid as we show in the problem scheme in figure 2.

The rigid body geometry is defined by:

$$\frac{x'^2}{a^2} + \frac{y'^2}{b^2} + \frac{z'^2}{c^2} = 1 \quad (9)$$

where a , b and c are the three principal semi-axis length of the rigid body, and x' , y' , z' are the Cartesian coordinates in a frame fixed to the body. The ellipse description from equation 9 is obtained for $c \rightarrow \infty$. The rigid body spatial orientation is defined by the Euler angles ϕ , θ and ψ following the z, x, z rotational order.

The fluid domain in the ellipsoidal 3D test is a rectangular prism with L , H and W side lengths. The ellipse 2D test has a rectangular fluid domain with L and H side lengths as shown in figure 2.

The rigid body and the fluid domain centroids are initially coincident. The fluid and rigid body mass density are set equal with no resultant buoyancy forces.

In two parallel walls or edges we impose a uniform velocity U_w as shown in figure 2. On all the remaining walls or edges, periodic boundary conditions are applied. The Dirichlet velocity boundary conditions in non regular geometries are imposed by Mei *et al.* (2000) method.

The rigid body dynamics in a pure rotational problem is strongly influenced by the Reynolds number problem defined as (Aidun *et al.*, 1998; Qi & Luo, 2003):

$$Re = \frac{4 G a^2}{\nu} \quad (10)$$

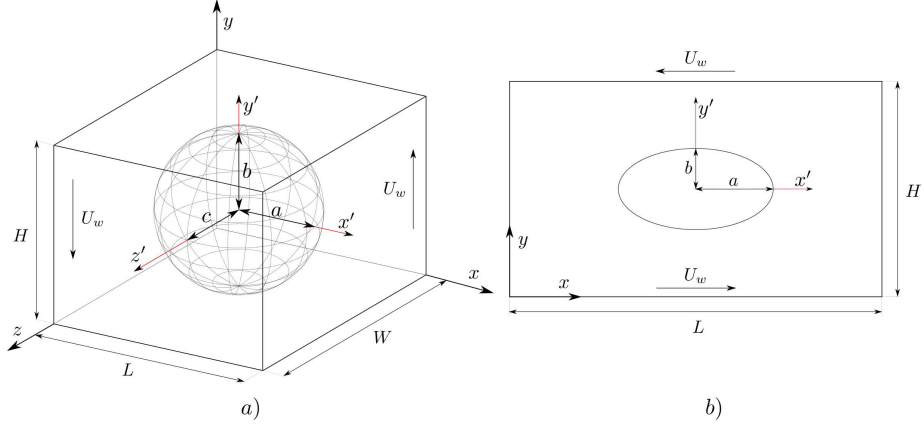


Figure 2: Schematic configuration of the rotational and orientational rigid body problem in Couette flow. Scheme a): free rotational ellipsoid in a 3D Couette flow, the fluid domain is a rectangular prism with side length L , H and W . We show the case $a = b = c$. Scheme b): free rotational ellipse in a 2D Couette flow in a rectangular domain with length L and H .

where $G = \frac{2U_w}{L}$ is the shear ratio and a is the major rigid body semi-axis. Some cautions should be taken when these results are compared with those in literature, because there are different definitions for G .

The dynamic of a rigid body immersed in a Couette flow has, as has been shown by Jeffery (1922), an analytical solution in the limit $Re \rightarrow 0$. The rigid body rotational velocity $\dot{\psi}$ about z' axis is determined from (Jeffery, 1922) by:

$$\dot{\psi} = \frac{G}{a^2 + b^2} (a^2 \cos^2(\psi) + b^2 \sin^2(\psi)) \quad (11)$$

where the rotational angle ψ is:

$$\psi = \tan^{-1} \left(\frac{b}{a} \tan \left(\frac{abGt}{a^2 + b^2} \right) \right) \quad (12)$$

This solution, valid to 2D and 3D (ellipse and ellipsoid) rotational problems in the limit $Re \rightarrow 0$, help us validating our LBM numerical results, which we present in the next sections.

3.2.1 Ellipse in Couette flow

In this test case we analyze the rotational behavior of an ellipse immersed in a Couette flow. In figure 2b) we show a schematic configuration of the ellipse and the fluid domain we use. We test the problem at two Reynolds numbers $Re = 0.032$ and $Re = 1.0$ and evaluate the results convergence to the problem's analytical solution presented in (Jeffery, 1922). The obtained

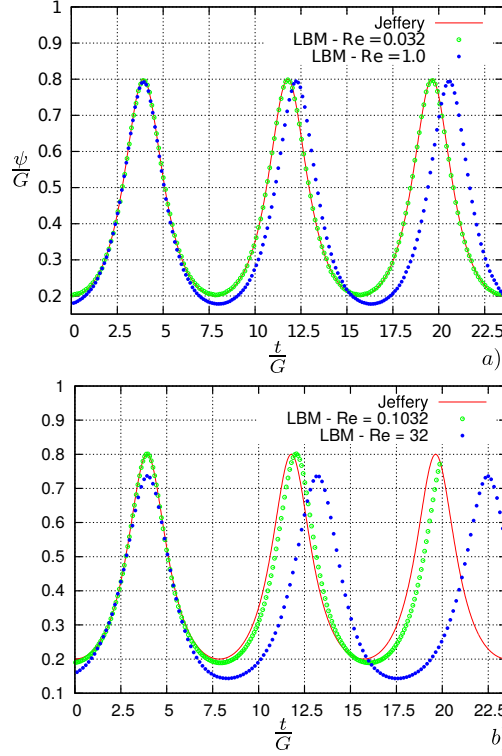


Figure 3: Ellipse and ellipsoid rotational angle ψ in fractions of shear ratio G at low Reynolds numbers. Figure a): ellipse rotational angle $\frac{\psi}{G}$ as function of $\frac{t}{G}$ at $Re = 0.032$ and $Re = 1.0$ compared with the Jeffery (1922) analytical solution at $Re \rightarrow 0$. The problem configuration is showed schematically in figure 2b). Figure b): ellipsoid rotational angle $\frac{\psi}{G}$ as function of $\frac{t}{G}$ at $Re = 0.1032$ and $Re = 32$ compared with the Jeffery (1922) analytical solution at $Re \rightarrow 0$. The problem configuration is showed schematically in figure 2a).

results are presented in figure 3a) along with the Jeffery analytical solution (equation 11).

The presented results are obtained with parameters $L = 0.8$ m and $H = 0.4$ m, and rigid body geometry defined by $a = 0.02$ m, and $b = \frac{a}{2}$. We impose a Dirichlet velocity boundary condition at the walls, where we set $U_w = 1.0$ m/s as we show in figure 2. To achieve the desired Reynolds number we choose an appropriate kinematic viscosity ν .

For the test at $Re = 0.032$ we set $\nu = 0.25$ m²/s and a domain discretization of 639×320 lattice grid points; while for the test at $Re = 1.0$ we set $\nu = 0.08$ m²/s with a domain discretization of 835×412 .

The fluid flow problems are solved using a *D2Q9i* LBM with simple relaxation time (SRT).

The results presented in figure 3a) show convergence to the analytical solution when $Re \rightarrow 0$. It is possible to observe, from figure 3a), a highly sensitive dynamical rigid body behavior when the Re number increase. For the $Re = 1.0$ the results show considerable changes with respect to the results at $Re = 0.032$. In particular there is an increase in the rotational period and a decrease in the lower rotational velocity for $Re = 1.0$ in comparison with those at $Re = 0.032$. In both problems we observe a periodic dynamical behavior as expected.

The obtained results for the rotational behavior of an ellipse in Couette flow are thus in agreement with those presented in Aidun *et al.* (1998) which shows the correctness of our algorithm to solve 2D pure rotational problems.

3.2.2 Ellipsoid in a Couette flow

We study here the rotational behavior of an ellipsoid immersed in a Couette flow, and compare the results with the analytical solution of Jeffery (1922). Figure 2a) shows a scheme of the geometry and fluid domain configuration for this problem.

Our LBM results are showed in figure 3b), obtained for Reynolds numbers $Re = 0.103$ and $Re = 32$, along with the Jeffery's analytical solution (see equation 11).

The parameters in our computations are $L = H = W = 0.1$ m (see figure 2a)). The ellipsoidal geometry is defined in equation 9 with $a = 0.025$ m, $b = c = \frac{a}{2}$, and the initial rigid body orientation is $\phi_0 = \theta_0 = \psi_0 = 0^\circ$.

The fluid domain is discretized by $64 \times 64 \times 64$ grid lattice points. We impose a constant velocity $U_w = 1.0$ m/s in the walls parallel to planes $x = 0$ and $x = L$ as we shown in figure 2a).

The kinematic viscosity is set to get the desired Reynolds numbers, and we use the *D3Q19i* simple relaxation time lattice Boltzmann model. We also test the problem using a *D3Q15i* lattice Boltzmann model and we do not find appreciable differences with the results obtained using *D3Q19i*.

From the results in figure 3b) we can see that the LBM results converge to the Jeffery (1922) analytical solution when $Re \rightarrow 0$. Our results for the rotational behavior of an ellipsoid in Couette flow agree with those presented in Aidun *et al.* (1998); Qi & Luo (2003); which shows the correctness of our algorithm to solve 3D pure rotational problems.

4 Ice crystals sedimentation in the atmosphere

In this section we study the main problem of this paper; we solve and analyze the dynamics of ice crystals sedimentation in the atmosphere. In particular, we are interested in evaluate the ice crystal settling velocity by using LBM for different ice crystal shapes in a range of size and mass.

The sedimentation of an ice crystal in the atmosphere is a fluid mechanical problem we model as follows. The crystal is considered a rigid body that moves under the action of its own weight, the buoyancy force and interacting only with the fluid that surrounds it. A simplifying assumption is adopted: no interactions between rigid bodies is considered. We are only interested in the dynamics of isolated rigid bodies in the atmosphere. This assumption is a good approximation to the movement of ice crystals in a cloud, since the concentration of ice particles in cirrus typically ranges between 50 and 500 liter⁻¹, while the maximum ice particle concentrations in cumulonimbus clouds reached 300 liter⁻¹ (Pruppacher *et al.*, 1998).

The dynamics of ice crystals of two shapes is analyzed, simple columns and six bullet-rosette polycrystals. In both cases the settling velocity is determined for several characteristic lengths.

The obtained LBM results are compared with some well known experimental data in literature (Jayaweera & Ryan, 1972; Kajikawa, 1973; Michaeli, 1977; Bürgesser *et al.*, 2016), as much as with the theoretical proposals from (Mitchell, 1996; Mitchell & Heymsfield, 2005; Khvorostyanov & Curry, 2002, 2005) and Westbrook (2008).

With the intention to be clear, in the next sections we present separately the obtained LBM results for both geometrical configurations.

4.1 Columnar ice crystals

In this section we present the settling velocity v_c results for sedimentation of columnar ice crystals in atmosphere obtained by using LBM. We compare these results with those obtained by experimental and theoretical methods well known in the literature.

Columnar ice crystals with quasi-hexagonal cross section and needle ice crystals, typically grown at temperatures between -3 and -9°C , have also been observed below -22°C (Magono & Lee, 1966; Ryan *et al.*, 1976; Heymsfield & Platt, 1984; Westbrook, 2008; Bailey & Hallett, 2009).

In our simulations the ice crystals are modeled by columns of hexagonal cross section, and the sedimentation studied in fluid flow regimes with $0.02 < Re < 0.25$. This is approximately the flow regime where the smallest particle can fall in a cloud. We adopt $d = \sqrt{l^2 + (2a)^2}$ as the length reference to evaluate the Reynolds number, where l is the ice crystal length and a is the semi-length of its cross section.

We perform numerical tests for a variety of aspect ratios $a_r = \frac{l}{2a} \in [1, 3]$. The length of the columnar ice crystals analyzed are in the range $16\mu\text{m} \leq l \leq 80\mu\text{m}$. The fluid properties are set as those at temperature $T = -8^\circ\text{C}$ with an atmospheric pressure $P = 101325\text{Pa}$. We have selected these fluid properties to simulate the atmospheric laboratory conditions used in Bürgesser *et al.* (2016).

The ice density for columns are set in the range reported by (Ryan *et al.*,

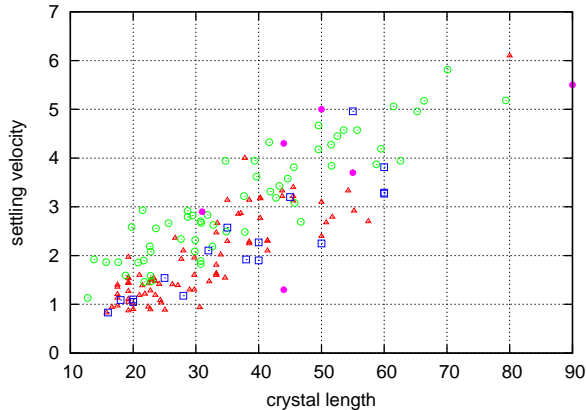


Figure 4: Settling velocity v_c for columnar ice crystals as a function of their length l . The showed results correspond to $a_r \in [1, 2]$. Velocity is expressed in centimeters per second cm/s, space in micrometers μm . The LBM results are showed with squares (\square). The experimental results are represented with: triangles (\triangle) for data from Bürgesser *et al.* (2016), hollow circles (\circ) for Kajikawa (1973) data, and with filled circles (\bullet) for Jayaweera & Ryan (1972) data.

1976) for $T = -8^\circ\text{C}$. It is also possible to obtain the ice crystal mass from relationships like those shape based proposed by (Mitchell, 1996).

In the figures 4 and 5 we show the settling velocity we obtained using LBM in comparison with the laboratory experimental results presented by Jayaweera & Ryan (1972); Kajikawa (1973); Bürgesser *et al.* (2016) as a function of crystals length. In the figure 4, LBM and experimental results are presented for aspect ratios between 1 and 2; while in the figure 5 comparative results for aspect ratios between 2 and 3 are showed. The presented LBM results were obtained for hexagonal columns in a variety of orientations and with different ice densities chosen from (Ryan *et al.*, 1976) for $T = -8^\circ\text{C}$.

As can be observed in the figures 4 and 5, the LBM results are in accordance with laboratory measurements. The results from Jayaweera & Ryan (1972); Kajikawa (1973); Bürgesser *et al.* (2016) present some dispersion as expected for a set of experimental data. For the length range and aspect ratio analyzed, all the numerical results are included in the data dispersion.

In the figure 6 the settling velocities obtained by LBM are shown in comparison with laboratory measurements presented in (Bürgesser *et al.*, 2016) as a function of crystals capacitance C . This parameter depends on the particle geometry and is obtained in Westbrook *et al.* (2008) for different geometries. For hexagonal columns the capacitance is:

$$C = 0.58a (1 + 0.95a_r^{0.75}) \quad (13)$$

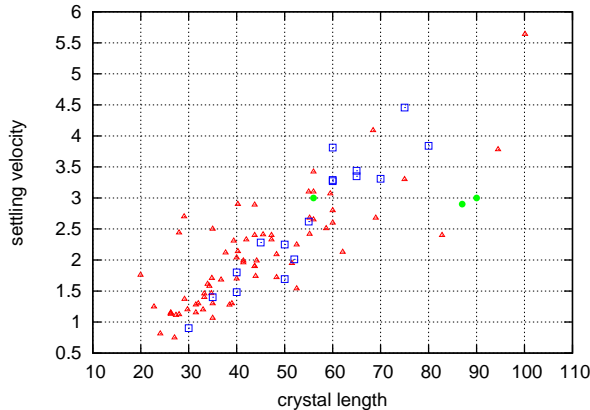


Figure 5: Settling velocity v_c for columnar ice crystals as a function of the length l . The showed results correspond to $a_r \in [2, 3]$. Velocity is expressed in centimeters per second cm/s, space in micrometers μm . The LBM results are showed with squares (\square). The experimental results are represented with: triangles (\triangle) for data from Bürgesser *et al.* (2016), and with filled circles (\bullet) for Jayaweera & Ryan (1972) data.

The numerical results are in the regime which allow us to compare with the measurements presented in Bürgesser *et al.* (2016), where they choose C as the characteristic length to evaluate the Reynolds number. The Reynolds number regime of the LBM results is $0.005 < Re < 0.1$ if we take C as the characteristic length.

It is possible to observe from the figure 6 that the dispersion of the LBM results have a notable decrease when the capacitance is used as variable. The same observation was pointed out by (Bürgesser *et al.*, 2016) for the experimental results. We can also observe from figure 6 that the results obtained with LBM are not uniformly distributed within the region containing experimental data. A bias towards the low part in this region can be seen. A bigger amount of computation would allow us to adjust a curve to the LBM results, though this is out of the scope of this work.

In the figure 7 we show the normalized falling velocity v_n obtained by LBM in comparison with some well known theoretical and experimental results from the literature. These results are the same we have presented for hexagonal columns but in a normalized way. The normalized velocity is computed as proposed by Westbrook (2008), this is, to obtain v_n , the crystal settling velocity v_c is divided by a sedimentation velocity v_r for an “equivalent sphere”. Here, equivalent sphere means a sphere with diameter $d = \sqrt{l^2 + (2a)^2}$ and mass m_s equal to the ice crystal mass m_{ic} . Westbrook (2008), based in results from Hubbard & Douglas (1993), propose an expression for v_c using the Stokes (White, 2005) solution for a sphere in a viscous

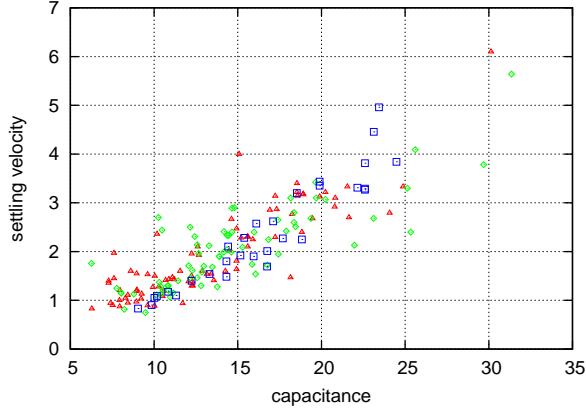


Figure 6: Settling velocity v_c for columnar ice crystals as a function of the capacitance C . Velocity is expressed in centimeters per second cm/s and distances in micrometers μm . The LBM results are showed with squares (\square). The experimental data from Bürgesser *et al.* (2016) are represented as: triangles \triangle , for aspect ratios between 1 and 2, and diamonds \diamond for aspect ratios between 2 and 3.

flow where the sphere radius is replaced by an effective hydrodynamic radius proportional to the capacitance C .

The dashed line in the figure 7 is the theoretical proposal presented by Westbrook (2008) to the normalized falling velocity. This proposal is formulated for columnar ice crystals with hexagonal cross section in random orientation. The results labeled as MHKC in the figure 7 correspond to the proposals from Mitchell (1996); Mitchell & Heymsfield (2005); Khvorostyanov & Curry (2002, 2005) in random orientation. MHKC is a typical nomenclature in literature to reference this group of methods. These are considered identical for $Re < 100$ (Heymsfield & Westbrook, 2010). Also we select from the literature and show in figure 7 some experimental data presented by Jayaweera & Ryan (1972); Kajikawa (1973); Michaeli (1977).

The LBM results at $0.01 < Re < 0.26$ ($0.005 < Re < 0.1$ with C as characteristic length) in the figure 7 are close and slightly above to the Westbrook (2008) theoretical proposal for hexagonal columns in random orientation. As expected from the previous comparison with experimental data, the LBM results in the figure 7 are below the MHKC proposals. The LBM results placed further above than Westbrook (2008) proposal belong to ice crystals falling in vertical or approximately vertical orientation.

The LBM results are obtained using a computational fluid domain as we have shown in the figure 1 with a relation $\frac{H}{L} \geq 12$. A $D3Q15i$ lattice Boltzmann model was used to obtain the numerical results. Using models with more velocities ($D3Q19$ or $D3Q27$), more accuracy can be obtained at a higher computational cost. Nevertheless, as shown in section 3, the

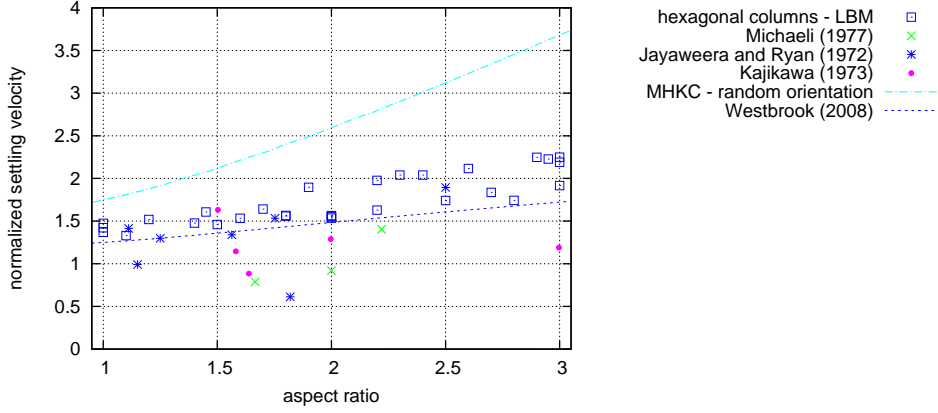


Figure 7: Normalized settling velocity v_n for hexagonal columns in function of ice crystals aspect ratio a_r . The dashed line shows the normalized terminal velocity proposed in Westbrook (2008) for a random orientation ice crystals. The experimental results are presented like those in Westbrook (2008).

D3Q15i model give acceptable (precise enough) results with a moderate computational cost. We use a grid refinement scheme with three to five grid scales along the longitudinal axis of the fluid domain.

The boundary conditions in the fluid domain are assigned as: free slip on vertical walls; Dirichlet constant velocity on the bottom wall; and convective boundary condition (as presented in section 2.2.1) on the top wall.

The fluid dynamics was computed in a fluid domain that moves with constant velocity. We use an initialization procedure as explained in section 3.1. Therefore, there is a fictitious transient movement which we are not interested in.

The presence of near free slip walls may have a minor but not negligible influence in the numerical falling velocity. These weak blockage effects are similar to those tested in section 3.1.

For blockage ratios (defined here as w/d) bigger than certain value, corrections should be applied to the results of numerical simulations. We observe that for blockage ratios smaller than 5.5% the influence of the walls is negligible. This maximum acceptable blockage value was obtained by evaluating the interference effects on a sphere in sedimentation. These interference effects are quantified by the relation between the LBM obtained settling velocity and that obtained from theoretical estimations in an unrestricted domain. Differences less than 0.5% between these velocities were observed for $w/d = 0.055$.

The computed results shown in this paper were obtained with blockage ratios smaller than 5.5%. This configuration allow us to get v_n by numerical evaluation of v_c and with v_r obtained from Stokes equation.

For particles in the analyzed Reynolds number regime we have not observed a preferential orientation. The observed crystal behaviors are in accordance with the results presented by Katz (1998), and with the experimental observations in Bürgesser *et al.* (2016). Katz (1998) has pointed out some behaviors about orientation of falling bodies at low Re . From experiments and theoretical predictions, he notes that needles will fall with indeterminate orientation in the limit $Re \rightarrow 0$. Also, at small but finite Re there will be an aligning torque tending to make its long axes horizontal.

To prove these results at small but finite Re , a number of numerical test were made in the regime $Re \approx 1$. For cylindrical particles in this regime its long axes keep approximately horizontal or a few degrees around this orientation. To check this preference orientation, we also made numerical tests with particles whose long axes are initially in a vertical orientation. The result we observe is that the particles always turn its long axes to an approximately horizontal orientation.

4.2 Six bullet-rosette ice polycrystals

This section presents the obtained falling velocity v_c results for ice polycrystals sedimentation. The geometry type of the analyzed ice polycrystals is the six bullet-rosette. A schematic geometrical configuration is shown in the figure 8 *a*).

Bullets and bullet-rosettes are polycrystals found in a variety of configurations and orientations in cirrus cloud (Heymsfield & Iaquinta, 2000; Westbrook *et al.*, 2008; Bailey & Hallett, 2009). Heymsfield & Iaquinta (2000) presented polycrystals habit percentages and a classification in shape and size in cirrus clouds as a function of temperature. Heymsfield & Platt (1984) found that bullet rosettes were the predominant form above -40°C in a mid-latitude cirrus cloud. Bailey & Hallett (2009) noted that bullet rosettes were typically observed between -40°C and -55°C .

There are different bullet-rosette models, Heymsfield & Iaquinta (2000) use 19-bullet rosette configuration in their study. We are interested in polycrystals with six hexagonal bullets placed at 90°C from each others. These polycrystal geometries are known as six bullet-rosette (or 6-rosette) in the literature.

The geometrical models used to represent the ice polycrystals are built by six arms of length l and diameter $2a$. The characteristic length of the polycrystals we analyze are in a range $l = 30 - 40 \mu\text{m}$. The arms are represented by hexagonal columns. These arms are joined together from one of its ends and placed at 90°C from each others as shown the figure 8 *a*). The polycrystal aspect ratio is defined as relative to the columnar length, $a_r = \frac{l}{2a}$. The analyzed models are a slight variation of those presented in Westbrook *et al.* (2008); Westbrook (2008); Heymsfield & Iaquinta (2000).

A bullet density of 0.81 gr/cm^3 is used as recommended in Heymsfield & Iaquinta

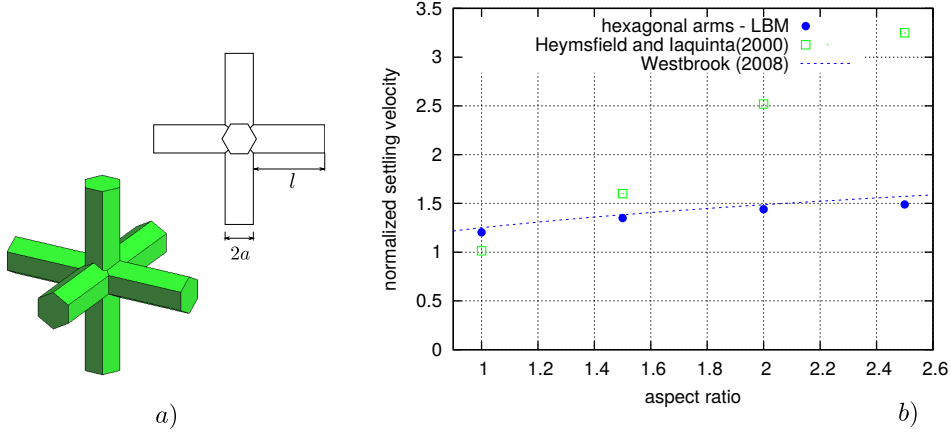


Figure 8: Figure *a*): schematic model used to represent the 6 bullet-rosette ice polycrystal. Figure *b*): normalized settling velocity v_n as a function of the crystal aspect ratio a_r . The figure also shows the normalized terminal velocity proposed in Westbrook (2008) for 6 bullet-rosette ice polycrystal, and the proposal from Heymsfield & Iaquina (2000) for the settling velocity of bullet-rosette with $d < 600 \mu\text{m}$.

(2000). The fluid properties are as those at $T = -40^\circ\text{C}$ in an international standard atmosphere (ISA).

The obtained LBM results and the normalized velocity v_n as proposed by Westbrook (2008), are shown in the figure 8 *b*). The v_n is obtained by dividing the six bullet-rosette settling velocity v_c by the terminal falling velocity v_r for an equivalent sphere. Where equivalent sphere means an sphere with diameter $d = 2(l + a)$ and mass m_s equal to the ice polycrystal mass m_{ic} .

The figure 8 *b*) shows the LBM results for aspect ratios between 1 and 2.5. The analyzed fluid mechanical problems are in a pure viscous regime at $0.075 < Re < 0.15$.

To compare with our results, we show in dashed line a theoretical proposal by Westbrook (2008) for six bullet-rosette polycrystal. Also we show an estimation from Heymsfield & Iaquina (2000) for the falling velocity of bullet-rosette with $d < 600 \mu\text{m}$. To the knowledge of the author, there are not available experimental measurement of falling velocity for the six-bullet ice polycrystals.

As can be observed in the figure, the numerical results are close and slightly below to those from the Westbrook (2008) proposal. One of the reasons of the noticeable gap between LBM results and Westbrook (2008) proposal may be the geometrical differences in the polycrystal model. It can be observed from the figure 8 *b*) that the Heymsfield & Iaquina (2000) proposal overestimate the falling velocity for $a_r > 1.5$ in comparison with

Westbrook (2008) and LBM results.

The LBM normalized vertical velocity in the figure 8 *b*) were obtained as in section 4.1 for columnar ice crystals.

5 Conclusion and discussion

We present in this work a Lattice-Boltzmann method to determine the dynamics of ice crystals in the atmosphere. Given a characterization for the shape, size and mass density of the crystals, together with its atmospheric habitat, it is possible to completely determine the dynamical behavior of the crystals. The numerical method proposed provides good results for the sedimenting velocity for the geometries, sizes and range of Reynolds number analyzed.

The LBM method takes into account the real geometry of the crystals. No approximations, as those proposed by Böhm (1989) and (Mitchell, 1996) which are widely used in the literature, are needed.

For the hexagonal column crystals, the results obtained by LBM are completely inside the dispersion region of the experimental, laboratory, measurements. When the capacitance (eq. 13, (Westbrook *et al.*, 2008)) is used as variable, the dispersion of both experimental and LBM results decreases noticeable. In this case a small bias of the LBM results towards the lower end of the dispersion region can be observed.

The amount of LBM computations done for this work is not enough to performs good curve fitting (which is not the goal of this work).

By direct comparison, we see that the LBM computed sedimenting velocity turns out to be a little higher than the Westbrook (2008) proposal, and much lower than the proposal of MHKC (proposals from Mitchell (1996); Mitchell & Heymsfield (2005); Khvorostyanov & Curry (2002, 2005)). This is observed for all the aspect ratios analyzed. The bigger differences we find with the proposal of Westbrook (2008) occur for columns with vertical or near vertical alignment.

In the problem of the six bullet rosette crystals the LBM results turn out to be very close and slightly below to the proposal of Westbrook (2008). The difference in the models used to represent the geometry of the crystals could be the reason for this slight difference. To the best of the author's knowledge, there are no reported experimental results for polycrystals of the size, shape and in the Reynolds regime analyzed.

We want to emphasize that a great deal of problems, with different geometries and values of parameters (like density, aspect ratio, etc.) can be analyzed by using the LBM methods. In this way one could get statistical characterizations, as those obtained via laboratory experiments, for new crystal shapes; one could also study the sensitivity models parameters, etc.

The author wants to thank Nesvit E. Castellano, Rodrigo E. Bürgesser

and Omar E. Ortiz for useful discussions and contributions. N. E. Castellano and R. E. Bürgesser brought the author’s attention to this subject. J. P. Giovacchini is a fellowship holder of CONICET (Argentina). This work was supported in part by grants 05-B454 of SECyT, UNC and PIDDEF 35/12 (Ministry of Defense, Argentina).

References

- AIDUN, CYRUS K. & LU, YANNAN 1995 Lattice boltzmann simulation of solid particles suspended in fluid. *Journal of Statistical Physics* **81** (1-2), 49–61.
- AIDUN, CYRUS K. & CLAUSEN, JONATHAN R. 2010 Lattice-boltzmann method for complex flows. *Annual Review of Fluid Mechanics* **42** (1), 439–472.
- AIDUN, CYRUS K., LU, YANNAN & DING, E.-JIANG 1998 Direct analysis of particulate suspensions with inertia using the discrete boltzmann equation. *Journal of Fluid Mechanics* **373**, 287–311.
- BAILEY, MATTHEW P. & HALLETT, JOHN 2009 A comprehensive habit diagram for atmospheric ice crystals: Confirmation from the laboratory, airs ii, and other field studies. *Journal of the Atmospheric Sciences* **66** (9), 2888–2899, arXiv: <http://dx.doi.org/10.1175/2009JAS2883.1>.
- BHATNAGAR, P. L., GROSS, E. P. & KROOK, M. 1954 A model for collision processes in gases. i. small amplitude processes in charged and neutral one-component systems. *Phys. Rev.* **94**, 511–525.
- BÖHM, JOHANNES P. 1989 A general equation for the terminal fall speed of solid hydrometeors. *Journal of the Atmospheric Sciences* **46** (15), 2419–2427.
- BÖHM, JOHANNES PETER 1992 A general hydrodynamic theory for mixed-phase microphysics. part i: drag and fall speed of hydrometeors. *Atmospheric Research* **27** (4), 253 – 274.
- BOUZIDI, MHAMED, FIRDAOUSS, MOUAOUIA & LALLEMAND, PIERRE 2001 Momentum transfer of a boltzmann-lattice fluid with boundaries. *Physics of Fluids* **13** (11), 3452–3459.
- BÜRGESSER, RODRIGO E., ÁVILA, ELDO E. & CASTELLANO, NESVIT E. 2016 Laboratory measurements of sedimentation velocity of columnar ice crystals. *Quarterly Journal of the Royal Meteorological Society* .

- CHIKATAMARLA, S. S., ANSUMALI, S. & KARLIN, I. V. 2006 Grad's approximation for missing data in lattice boltzmann simulations. *EPL (Europhysics Letters)* **74** (2), 215.
- EIDHAMMER, T., MORRISON, H., BANSEMER, A., GETTELMAN, A. & HEYMSFIELD, A. J. 2014 Comparison of ice cloud properties simulated by the community atmosphere model (cam5) with in-situ observations. *Atmospheric Chemistry and Physics* **14** (18), 10103–10118.
- FAKHARI, ABBAS & LEE, TAEHUN 2014 Finite-difference lattice boltzmann method with a block-structured adaptive-mesh-refinement technique. *Phys. Rev. E* **89**, 033310.
- FILIPPOVA, O. & HNEL, D. 1998*a* Boundary-fitting and local grid refinement for lattice-bgk models. *International Journal of Modern Physics C* **09** (08), 1271–1279.
- FILIPPOVA, OLGA & HNEL, DIETER 1998*b* Grid refinement for lattice-bgk models. *Journal of Computational Physics* **147** (1), 219 – 228.
- GIOVACCHINI, JUAN P. & ORTIZ, OMAR E. 2015 Flow force and torque on submerged bodies in lattice-boltzmann methods via momentum exchange. *Phys. Rev. E* **92**, 063302.
- GOLDSTEIN, HERBERT, POOLE, CHARLES P. & SAFKO, JOHN L. 2001 *Classical Mechanics*, 3rd edn. Addison-Wesley.
- HARRIS, S. 2004 *An Introduction to the Theory of the Boltzmann Equation*. *Dover books on physics*. Dover Publications.
- HE, XIAOYI & LUO, LI-SHI 1997*a* Lattice boltzmann model for the incompressible navierstokes equation. *Journal of Statistical Physics* **88** (3-4), 927–944.
- HE, XIAOYI & LUO, LI-SHI 1997*b* Theory of the lattice boltzmann method: From the boltzmann equation to the lattice boltzmann equation. *Phys. Rev. E* **56** (6), 6811–6817.
- HEYMSFIELD, ANDREW J. & IAQUINTA, JEAN 2000 Cirrus crystal terminal velocities. *Journal of the Atmospheric Sciences* **57** (7), 916–938.
- HEYMSFIELD, ANDREW J. & PLATT, C. M. R. 1984 A parameterization of the particle size spectrum of ice clouds in terms of the ambient temperature and the ice water content. *Journal of the Atmospheric Sciences* **41** (5), 846–855, arXiv: [http://dx.doi.org/10.1175/1520-0469\(1984\)041<0846:APOTPSj2.0.CO;2](http://dx.doi.org/10.1175/1520-0469(1984)041<0846:APOTPSj2.0.CO;2).

- HEYMSFIELD, A. J. & WESTBROOK, C. D. 2010 Advances in the estimation of ice particle fall speeds using laboratory and field measurements. *Journal of the Atmospheric Sciences* **67** (8), 2469–2482.
- HUBBARD, JOSEPH B. & DOUGLAS, JACK F. 1993 Hydrodynamic friction of arbitrarily shaped brownian particles. *Phys. Rev. E* **47**, R2983–R2986.
- INAMURO, TAKAJI, MAEBA, KOJI & OGINO, FUMIMARU 2000 Flow between parallel walls containing the lines of neutrally buoyant circular cylinders. *International Journal of Multiphase Flow* **26** (12), 1981 – 2004.
- JAYAWEERA, K. O. L. F. & COTTIS, R. E. 1969 Fall velocities of plate-like and columnar ice crystals. *Quarterly Journal of the Royal Meteorological Society* **95** (406), 703–709.
- JAYAWEERA, K. O. L. F. & RYAN, B. F. 1972 Terminal velocities of ice crystals. *Quarterly Journal of the Royal Meteorological Society* **98** (415), 193–197.
- JEFFERY, G. B. 1922 The motion of ellipsoidal particles immersed in a viscous fluid. *Proceedings of the Royal Society of London A: Mathematical, Physical and Engineering Sciences* **102** (715), 161–179.
- JUNK, MICHAEL & YANG, ZHAOXIA 2008 Outflow boundary conditions for the lattice boltzmann method. *Progress in Computational Fluid Dynamics* **8** (1-4), 38–48.
- KAJIKAWA, M. 1973 Laboratory measurement of falling velocity of individual ice crystals. *Meteorological Society of Japan. Journal. Ser.II* **Vol. 51** (no. 4), P.263–272, 7 refs. CRREL Acc. No: 28002698.
- KATZ, J. I. 1998 Subsuns and low reynolds number flow. *Journal of the Atmospheric Sciences* **55** (22), 3358–3362, arXiv: [http://dx.doi.org/10.1175/1520-0469\(1998\)055<3358:SALRNF;2.0.CO;2](http://dx.doi.org/10.1175/1520-0469(1998)055<3358:SALRNF;2.0.CO;2).
- KHVOROSTYANOV, VITALY I. & CURRY, JUDITH A. 2002 Terminal velocities of droplets and crystals: Power laws with continuous parameters over the size spectrum. *Journal of the Atmospheric Sciences* **59** (11), 1872–1884.
- KHVOROSTYANOV, VITALY I. & CURRY, JUDITH A. 2005 Fall velocities of hydrometeors in the atmosphere: Refinements to a continuous analytical power law. *Journal of the Atmospheric Sciences* **62** (12), 4343–4357, arXiv: <http://dx.doi.org/10.1175/JAS3622.1>.
- LADD, ANTHONY J. C. 1994a Numerical simulations of particulate suspensions via a discretized boltzmann equation. part 1. theoretical foundation. *Journal of Fluid Mechanics* **271**, 285–309.

- LADD, ANTHONY J. C. 1994*b* Numerical simulations of particulate suspensions via a discretized boltzmann equation. part 2. numerical results. *Journal of Fluid Mechanics* **271**, 311–339.
- LAGRAVA, D., MALASPINAS, O., LATT, J. & CHOPARD, B. 2012 Advances in multi-domain lattice boltzmann grid refinement. *Journal of Computational Physics* **231** (14), 4808 – 4822.
- LI, HUABING, LU, XIAOYAN, FANG, HAIPING & QIAN, YUEHONG 2004 Force evaluations in lattice boltzmann simulations with moving boundaries in two dimensions. *Phys. Rev. E* **70**, 026701.
- LOCATELLI, JOHN D. & HOBBS, PETER V. 1974 Fall speeds and masses of solid precipitation particles. *Journal of Geophysical Research* **79** (15), 2185–2197.
- MAGONO, CHOJI & LEE, CHUNG WOO 1966 Meteorological classification of natural snow crystals. *Journal of the Faculty of Science, Hokkaido University. Series 7, Geophysics* **2** (4).
- MEI, RENWEI, LUO, LI-SHI & SHYY, WEI 1999 An accurate curved boundary treatment in the lattice boltzmann method. *Journal of Computational Physics* **155** (2), 307 – 330.
- MEI, RENWEI, SHYY, WEI, YU, DAZHI & LUO, LI-SHI 2000 Lattice boltzmann method for 3-d flows with curved boundary. *Journal of Computational Physics* **161** (2), 680 – 699.
- MEI, RENWEI, YU, DAZHI, SHYY, WEI & LUO, LI-SHI 2002 Force evaluation in the lattice boltzmann method involving curved geometry. *Phys. Rev. E* **65**, 041203.
- MICHAELI, GABRIEL 1977 Settling velocities of small ice crystals. *Tellus* **29** (3), 282–285.
- MITCHELL, DAVID L. 1996 Use of mass- and area-dimensional power laws for determining precipitation particle terminal velocities. *Journal of the Atmospheric Sciences* **53** (12), 1710–1723.
- MITCHELL, DAVID L. & HEYMSFIELD, ANDREW J. 2005 Refinements in the treatment of ice particle terminal velocities, highlighting aggregates. *Journal of the Atmospheric Sciences* **62** (5), 1637–1644.
- MIYAMURA, A., IWASAKI, S. & ISHII, T. 1981 Experimental wall correction factors of single solid spheres in triangular and square cylinders, and parallel plates. *International Journal of Multiphase Flow* **7** (1), 41 – 46.

- PRUPPACHER, HANS R., KLETT, JAMES D. & WANG, PAO K. 1998 Microphysics of clouds and precipitation. *Aerosol Science and Technology* **28** (4), 381–382, arXiv: <http://dx.doi.org/10.1080/02786829808965531>.
- QI, DEWEI & LUO, LI-SHI 2003 Rotational and orientational behaviour of three-dimensional spheroidal particles in couette flows. *Journal of Fluid Mechanics* **477**, 201–213.
- RYAN, B. F., WISHART, E. R. & SHAW, D. E. 1976 The growth rates and densities of ice crystals between $3C^{\circ}$ and $21C^{\circ}$. *Journal of the Atmospheric Sciences* **33** (5), 842–850.
- SOHANKAR, A., NORBERG, C. & DAVIDSON, L. 1998 Low-reynolds-number flow around a square cylinder at incidence: study of blockage, onset of vortex shedding and outlet boundary condition. *International Journal for Numerical Methods in Fluids* **26** (1), 39–56.
- SONE, Y. 2007 *Molecular Gas Dynamics: Theory, Techniques, and Applications. Modeling and Simulation in Science, Engineering and Technology*. Springer London, Limited.
- SUCCI, SAURO 2001 *The lattice Boltzmann equation for fluid dynamics and beyond. Numerical Mathematics and Scientific Computation*. Oxford: Oxford University Press.
- TÖLKE, JONAS, FREUDIGER, SREN & KRAFCZYK, MANFRED 2006 An adaptive scheme using hierarchical grids for lattice boltzmann multi-phase flow simulations. *Computers & Fluids* **35** (89), 820 – 830, proceedings of the First International Conference for Mesoscopic Methods in Engineering and Science.
- WEN, BINGHAI, LI, HUABING, ZHANG, CHAOYING & FANG, HAIPING 2012 Lattice-type-dependent momentum-exchange method for moving boundaries. *Phys. Rev. E* **85**, 016704.
- WEN, BINGHAI, ZHANG, CHAOYING, TU, YUSONG, WANG, CHUNLEI & FANG, HAIPING 2014 Galilean invariant fluid-solid interfacial dynamics in lattice boltzmann simulations. *J. Comput. Phys.* **266**, 161–170.
- WESTBROOK, C. D. 2008 The fall speeds of sub-100 m ice crystals. *Quarterly Journal of the Royal Meteorological Society* **134** (634), 1243–1251.
- WESTBROOK, CHRISTOPHER DAVID, HOGAN, ROBIN J. & ILLINGWORTH, ANTHONY J. 2008 The capacitance of pristine ice crystals and aggregate snowflakes. *Journal of the Atmospheric Sciences* **65** (1), 206–219.
- WHITE, FRANK 2005 *Viscous Fluid Flow*. McGraw-Hill Education.

- WOLF-GLADROW, D.A. 2000 *Lattice-Gas Cellular Automata and Lattice Boltzmann Models: An Introduction. Lattice-gas Cellular Automata and Lattice Boltzmann Models: An Introduction* n.º 1725. Springer.
- XIA, ZHENHUA, CONNINGTON, KEVIN W., RAPAKA, SAIKIRAN, YUE, PENGTAO, FENG, JAMES J. & CHEN, SHIYI 2009 Flow patterns in the sedimentation of an elliptical particle. *Journal of Fluid Mechanics* **625**, 249–272.
- YANG, ZHAOXIA 2007 Analysis of lattice boltzmann boundary conditions. PhD thesis, Mathematisch-Naturwissenschaftliche Sektion Fachbereich Mathematik und Statistik - Universität Konstanz.
- YANG, ZHAOXIA 2013 Lattice boltzmann outflow treatments: Convective conditions and others. *Computers & Mathematics with Applications* **65** (2), 160 – 171, special Issue on Mesoscopic Methods in Engineering and Science (ICMMES-2010, Edmonton, Canada).
- YU, DAZHI, MEI, RENWEI & SHYY, WEI 2002 A multi-block lattice boltzmann method for viscous fluid flows. *International Journal for Numerical Methods in Fluids* **39** (2), 99–120.
- YU, DAZHI, MEI, RENWEI & SHYY, WEI 2005 Improved treatment of the open boundary in the method of lattice boltzmann equation: general description of the method. *Progress in Computational Fluid Dynamics, an International Journal* **5** (1), 3 – 12.
- ZOU, QISU & HE, XIAOYI 1997 On pressure and velocity boundary conditions for the lattice boltzmann bgk model. *Phys. Fluids E* **9** (6), 1591–1598.